Journal of Catalysis 377 (2019) 153–162

Contents lists available at ScienceDirect

Journal of Catalysis

journal homepage: www.elsevier.com/locate/jcat

Presituated "coke"-determined mechanistic route for ethene formation in the methanol-to-olefins process on SAPO-34 catalyst

Jibin Zhou [a,b,1], Yuchun Zhi [a,1], Jinling Zhang [a], Zhiqiang Liu [b,c], Tao Zhang [a], Yanli He [a], Anmin Zheng [c], Mao Ye [a,*], Yingxu Wei [a], Zhongmin Liu [a,*]

[a] National Engineering Laboratory for Methanol to Olefins, Dalian National Laboratory for Clean Energy, iChEM (Collaborative Innovation Center of Chemistry for Energy Materials), Dalian Institute of Chemical Physics, Chinese Academy of Sciences, Dalian 116023, People's Republic of China
[b] University of Chinese Academy of Sciences, Beijing 100049, People's Republic of China
[c] State Key Laboratory of Magnetic Resonance and Atomic and Molecular Physics, National Center for Magnetic Resonance in Wuhan, Wuhan Institute of Physics and Mathematics, Chinese Academy of Sciences, Wuhan 430071, People's Republic of China

ARTICLE INFO

Article history:
Received 26 December 2018
Revised 5 June 2019
Accepted 11 June 2019
Available online 30 July 2019

Keywords:
Methanol to olefins
SAPO-34
Pre-coking
"Coke" location
Ethene selectivity

ABSTRACT

Control of product selectivity is a central yet challenging issue in catalysis chemistry, both in academia and industry. The ever-increasing market demand for ethene, together with relatively low ethene selectivity, necessitates the upgrading of the current methanol-to-olefins (MTO) industry to enhance ethene selectivity. We report here an operable strategy, 1-butene "precoking" technology, by which ethene selectivity has been unprecedentedly enhanced while the catalyst lifespan has been conserved. We also made effects to provide more insight into the long-standing controversies regarding the mechanistic origin of the increase in ethene selectivity. With the aid of a ^{12}C-/^{13}C-methanol switch experiment, MD calculations, and FTIR analysis, it was demonstrated that ethene increase is neither simply—or solely—caused by the configurational diffusion effect, nor due to the transition-state shape selectivity or methylnaphthalene species, but rather to the spatial siting of the presituated "coke". The relatively evenly distributed presituated coke extends the reaction zone toward the near-core of the SAPO-34 crystal, elongating the diffusion trajectories of molecules and allowing more acid sites to be utilized. The diffusion-hindered higher olefinic intermediates tend to evolve to active aromatic species, which, in turn, lead substantially to ethene. This mechanistic understanding could be also applicable to explaining ethene increase with time on stream (TOS) on parent SAPO-34.

1. Introduction

Light olefins, traditionally produced from the cracking of naphtha, have been serving as an essential building block for the chemical industry. The MTO process, emerging as a promising nonoil pathway for light olefin production, has been commercialized recently [1]. This technology adopts a fluidized bed reactor–regenerator configuration, in which continuous catalyst circulation leads inevitably to an age distribution of catalysts in the reactor and concomitantly an uneven deposition of carbonaceous species on individual catalyst particles [1,2]. This nonuniform coking behavior of catalysts would average and, to be more specific, lower the overall ethene selectivity. Moreover, a common feature of the MTO reaction is rather lower initial ethene selectivity, which raises the issue that the "optimal operation window" is too narrow to maximize light olefins for industrial operation [1]. To circumvent these limitations, developing new strategies to enhance the initial ethene selectivity is highly desirable. Meanwhile, a thorough interpretation of the mechanistic origin of ethene increase holds practical significance as a fundamental basis for the MTO technology development.

It is generally accepted that the MTO reaction follows a dual-cycle mechanism consisting of olefins-based and aromatics-based cycles [3,4], involving successive methylation and cracking of retained active alkenes and aromatic species. The dual-cycle catalytic mechanism was initially proposed in the context of HZSM-5 zeolite [3,4] but was seldom invoked for cage-structured SAPO-34 [5]; it rationalizes the product distribution to a certain extent, with ethene being generated exclusively via the aromatics-based cycle and propene and other higher alkenes being produced from both pathways [3,4,6]. It should be recognized that this mechanistic genesis of ethene and propene was established at

* Corresponding authors.
E-mail addresses: maoye@dicp.ac.cn (M. Ye), liuzm@dicp.ac.cn (Z. Liu).
[1] Jibin Zhou and Yuchun Zhi contributed equally.

https://doi.org/10.1016/j.jcat.2019.06.014
0021-9517/

a lower reaction temperature of 350 °C, not relevant to the industrial conditions (usually above 450 °C). Yet, the methanol conversion mechanism and accordingly the induced product selectivities may vary significantly with catalysts [5,7,8], temperatures [7,8], TOS [5], and further applied conditions. Hence, any conclusion reached with respect to mechanistic issues must be very careful and consistent comparability of experimental results must be maintained.

The dual-cycle mechanism does not deal with the evolution of active hydrocarbon pool (HCP) species toward inactive ones. Nevertheless, the accumulation of inert carbonaceous deposits inside the cavities of SAPO-34 would impede the mass transfer and accessibility of active sites, but also may modulate the reaction trajectory by modifying the local catalytic environment. One remarkable consequence of the accumulated "coke" is the gradual increase in ethene selectivity as the reaction proceeds [1,2,9]. This ubiquitous phenomenon is important, as it suggests a potential approach to tailoring product selectivity. Our laboratory set out a few decades ago to develop "precoking" technology using a diverse set of hydrocarbons as "coke" precursors. A certain quantity of linear hydrocarbons and active aromatics were also retained inside the cages of SAPO-34 after reaction; to avoid misleading, we use "coke" or C-Retained [10,11] to replace the term *coke* in this work. To significantly enhance ethene selectivity without impairing the catalyst lifetime is a great challenge, since the formation of ethene is, in principle, associated with the buildup of aromatics which tend to evolve into more condensed ones, deactivating the catalyst [12]. To date, no clear mechanistic picture exists regarding the essential cause of the contributions of such "coke" or C-retained species, although substantial efforts have been devoted to addressing this issue [5,13–15]. It remains debatable as to whether the increase in ethene selectivity is a result of the product shape selectivity [5,14] or of the transition-state shape selectivity [12,15] or due to the abundance of methylnaphthalene species [16]. Another significant concern that prompts us to revisit this issue is that the chemical composition of the deposited soluble "coke" has been well identified and analyzed [17], while the spatial location of this "coke" distributed in an individual crystal and its connection with the product selectivity were scarcely examined [18].

In this contribution, we not only report a promising "precoking" technology exemplified by 1-butene cracking, by which the product selectivity of the MTO reaction has been effectively modulated toward ethene, but also provide insight into the long-standing controversies regarding the mechanistic origin of the increase in ethene selectivity. The "precoking" technology reported here can be realized readily by recycling the unwanted byproducts such as 1-butene from the MTO process itself. The 1-butene cracking ("precoking") process contributes to a certain amount of ethene as well.

2. Experimental

2.1. Catalyst and characterization

The industrial MTO catalyst mainly composed of the SAPO-34 molecular sieve was used in this work [1].

The crystallinity of catalysts was characterized by powder X-ray diffraction on a PANalytical X'Pert PRO X-ray diffractometer with CuKα radiation (λ = 1.54059 Å) at 40 kV and 40 mA.

Nitrogen adsorption–desorption measurements on catalysts were carried out in liquid nitrogen on a Micromeritics ASAP2020 setup. Prior to nitrogen sorption, the solid sample was degassed at 350 °C for 4 h under vacuum. The Brunauer–Emmett–Teller (BET) equation was applied to determine the specific surface area using the adsorption data in the range P/P_0 = 0.05–0.2. The *t*-plot method was used to calculate the external surface area, micropore area, and micropore volume using the adsorption data at P/P_0 = 0.2. The total pore volume was determined from the amount of nitrogen adsorbed at P/P_0 = 0.972 [19,20].

The "coke" amount of the "coked" catalyst was measured by thermogravimetric analysis (TGA) and analysis was carried out on an SDTQ 600 setup. Typically, the sample was heated from room temperature to 900 °C at a rate of 10 °C min^{-1} (under flowing air at 100 ml min^{-1}).

Diffuse reflectance infrared Fourier transform (DRIFT) spectra were measured on an FT-IR spectrometer (Tensor 27, Bruker). The catalyst was weighed exactly to ensure that the same amount was used for each sample. The sample was activated at 450 °C in N_2 for 2 h to remove the adsorbed water and then cooled down to 50 °C for measurement. The DRIFT spectra were recorded in the range 4000–600 cm^{-1} with a resolution of 4 cm^{-1}. The spectrum of KBr acquired under the same conditions was used as the background signal.

Acidity measurements were made by NH_3-IR spectroscopy using a Nicolet Magna FTIR 550 spectrometer (resolution 4 cm^{-1}). First, the samples were pressed into thin wafers and activated *in situ* in the IR cell under 10^{-2} Pa at 450 °C for 1 h. The IR spectra were then recorded at room temperature. NH_3 adsorption was carried out at room temperature for 0.5 h; then the spectra were recorded at 150 °C.

The retained soluble "coke" species were determined by the Guisnet method [21]. First, the spent catalyst (50 mg) was dissolved in 1.0 ml of 20% HF solution in a Teflon screwcap. Then, 1.0 ml CH_2Cl_2 with C_2Cl_6 as internal standard was added to extract the soluble "coke" which was subsequently analyzed and quantified by the GC–MS method. The GC–MS analysis was carried out by an Agilent 7890A gas chromatograph equipped with an Agilent 5795C mass-selective detector and a HP-5 capillary column (30 m, 0.25 mm i.d., stationary phase thickness 0.25 μm) and an FID detector. The retained lighter alkanes were captured by the modified "coke" extraction method. That is, the spent catalyst was first soaked in CH_2Cl_2 solvent for a while and then HF solution was added to digest the framework of the SAPO-34 crystal. Following this, the extracts were analyzed by the GC–MS method.

The uptake of methanol was performed on a gravimetric analyzer (IGA100, Hiden Isochema, Warrington, UK). The pressure was determined by two high-accuracy Baratron pressure transducers. About 50-mg samples were loaded into the microbalance bucket and outgassed under vacuum (<10^{-3} Pa) at 250 °C for 2 h prior to the sorption measurements. The adsorption isotherms were acquired at 50 °C under a maintained pressure of 10 mbar. The dosing of methanol was slow enough to keep the adsorption process isothermal. The dosing continued until the equilibrium adsorption isotherm was achieved.

2.2. Catalytic studies

2.2.1. "Precoking" and MTO reaction

Both the 1-butene "precoking" treatment and the following MTO reaction were carried out in a fluidized bed reactor with inner diameter of 0.019 m and height of 0.35 m under atmospheric pressure. The state of fluidization is crucial, as it affects the mass transfer. The particle size distribution (PSD), as shown in Section 3.1, showed that the particle size of the SAPO-34 catalyst was mainly 80–120 μm. The minimum fluidizing velocity (U_{mf}), depending on the particle size of the catalyst, is an important parameter and was calculated to be 6 mm/s. The minimum bubbling velocity (U_{mb}) was determined to be 1 cm/s, and the initial turbulence velocity was 0.4 m/s. However, the actual fluidizing velocity was 3 cm/s for the "precoking" reaction and 7 cm/s for the MTO reaction. Therefore, both the "precoking" and MTO reactions were

operated in a bubbling state. For a typical reaction, the catalyst was first activated at 550 °C for 30 min in nitrogen flow, and then 1-butene was fed into the reactor with a weight hour space velocity (WHSV) of 2 h^{-1} at 550 °C for "precoking" treatment for 2, 5, and 10 min, respectively. After the temperature was lowered to 490 °C, methanol solution (with 20 wt% water) was fed by a piston pump and passed through a vaporizer before entering the reactor with WHSV of 5 h^{-1}. The reaction products were analyzed by an online gas chromatograph (Agilent GC 7890N), equipped with an FID detector and a Plot-Q column. The conversion and selectivity for the MTO reaction were calculated on a CH_2 basis. Dimethyl ether was considered as a reactant in terms of the fast equilibrium between methanol and dimethyl ether.

2.2.2. ^{12}C-/^{13}C-methanol switch experiment

In the ^{12}C-/^{13}C-methanol switch experiments, first ^{12}C-methanol was fed into the reactor to build up ^{12}C-containing species for 2, 20, and 38 min at 490 °C in the fluidized bed reactor, and then the catalyst was quickly cooled and transferred to the fixed bed reactor for feeding ^{13}C-methanol at 490 °C for 10 s. After a predetermined time in terms of the delay time before the methanol reached the catalyst bed under the reaction conditions studied, the reactor was quickly cooled quickly with liquid nitrogen and then removed from the oven. The isotopic distribution of effluent was analyzed by the online GC–MS (Agilent 7890B/5977A). The confined aromatic species were obtained by HF dissolution followed by CH_2Cl_2 extraction as described in the section *Characterization of catalysts*. The isotopic distribution of the retained aromatics was analyzed by GC–MS (Agilent 7890A/5975C). It should be pointed out here that ^{12}C-/^{13}C-methanol switch experiments cannot be carried out solely in the fluidized bed reactor due to the limitations of practical operation. However, the results presented here are convincing, because the mass loss of the catalyst from being discharged from the fluidized bed reactor after the MTO reaction to being reheated to 490 °C in the fixed-bed reactor is small. In addition, we performed ^{12}C-/^{13}C-methanol switch experiments for SAPO-34-PC solely in a fixed-bed reactor, the isotopic distribution for the effluent and retained aromatics as shown in Fig. S1 in the Supplementary Material were found to be comparable with those obtained by the above-applied method (Section 3.6). This result further evidences the feasibility of the ^{12}C-/^{13}C-methanol switch experiments performed here.

2.2.3. Theoretical calculations

In our simulations, we neglect the acid sites and take the CHA-typed AlPO-34 as catalyst. The initial structure of pure siliceous zeolite was taken from the International Zeolite Associations database [22], subsequently Al and P atoms were substituted, and finally the structure was optimized by GULP [23] with an SLC core–shell force field [24]. The loading number was fixed at 27 for all the adsorbed molecules (ethene, propene, and 1-butene) and $3 \times 3 \times 3$ super cells was used in the subsequent molecular dynamics (MD) simulation (Fig. S2).

MD simulations were performed in the canonical ensemble (*NVT*), where the number of particles (*N*), simulation volume (*V*), and temperature (*T*) were kept constant. The simulated temperature was controlled by a Nosé–Hoover thermostat with a coupling time constant of 1 ps and held at 27, 290, and 490 °C, respectively. The velocity Verlet algorithm was used throughout to integrate Newton's equations of motion. A TraPPE [25] force field was used for ethene, propene, and 1-butene molecules. The parameters of the zeolite force field were given in the original reference by Rives [26]. All the Lennard–Jones cross-interaction parameters were determined by the Lorentz–Berthelot mixing rules, and the cutoff radius was 14 Å. Each MD simulation started with annealing and was followed by 5×10^6 with 1 fs timestep. Then a production run of 1×10^8 steps was performed. Three independent MD simulations were carried out for each system for better statistics. The trajectories were recorded every 1000 steps to analyze the diffusion coefficients. All MD was performed in the parallel general purpose DL_POLY_2.20 code [27].

The self-diffusion coefficient can be obtained by MD simulation. In this work, the mean square displacement (MSD) of an adsorbed molecule is defined as

$$MSD(\tau) = \frac{1}{N_m}\sum_{i}^{N_m}\frac{1}{N_\tau}\sum_{t_0}^{N_t}\left[r_i(t_0+\tau) - r_i(t_0)\right]^2 \quad (1)$$

where N_m is the number of adsorbed molecules, N_τ is the number of time origins used in calculating the average, and r_i is the coordinate of molecule *i*. In addition, the slope of the MSD as a function of time determines the self-diffusion coefficient, D_s, defined according to the so-called Einstein relation [28],

$$MSD(\tau) = 6D_s\tau + b \quad (2)$$

where *b* is the thermal factor arising from atomic vibrations. The line is fitted in the range 400–10,000 ps using a least-squares fit. The reported MSD curves and corresponding D_s values are calculated as the averages of three independent MD trajectories.

3. Results and discussion

3.1. Catalyst characterization

The crystal size of the applied SAPO-34 crystal determined by the PSD method was, on the average, around 6–7 μm (Fig. 1a). The particle size of the catalyst (shaped with binder) was around 80–120 μm (Fig. 1b). Other physicochemical properties (including XRD, surface area, pore volume, and acidity density) were tested and are compiled in Fig. S6, Table 1, and Table S2.

3.2. 1-Butene "precoking" reaction

The effluent product distribution of 1-butene cracking ("precoking") for different times over SAPO-34 at 550 °C is summarized in Table S1. It is seen that 1-butene cracking afforded ca. 10–17% ethene. Strikingly, the selectivity to C_5^+ products increased when 1-butene cracking time was prolonged from 2 to 10 min. This phenomenon was reported elsewhere without explanation [29]. It seemingly contrasts with the intuitive expectation that the cumulated C-Retained should hinder C_5^+ entities from diffusing out of the SAPO-34 cages [1,16,17]. However, considering that high temperature facilitates the migration of the reaction zone toward the inner part of the crystal [18] and the rather lower reactivity of light olefins relative to methanol [30,31], it appears rational to surmise that 1-butene molecules are able to diffuse toward the interior part of the crystal (at 550 °C), where HCP species are largely formed, while the bulkier C_5^+ products have great difficulty diffusing out of the crystal due to the diffusion hindrance. Afterward, the reaction zone moves steadily outward, favoring the escape of C_5^+ products. This proposed reaction pattern resembles the case of the conversion of ethene (rapidly formed via ethanol dehydration), where heavier HCP species were also initially formed in close proximity to the core of the SAPO-34 crystal [18]. If this was the case, the presituated "coke" resulting from 1-butene cracking would not concentrate at the periphery cages of SAPO-34 but would distribute relatively evenly throughout the crystal.

To discern whether or not highly active acid sites are present in the studied SAPO-34 and responsible for the "precoking" reaction, ^{29}Si MAS NMR techniques are applied here to assist in differentiating the Si environment of SAPO-34 crystallite. The NMR spectrum, as depicted in Fig. S3, shows a single sharp peak centered at

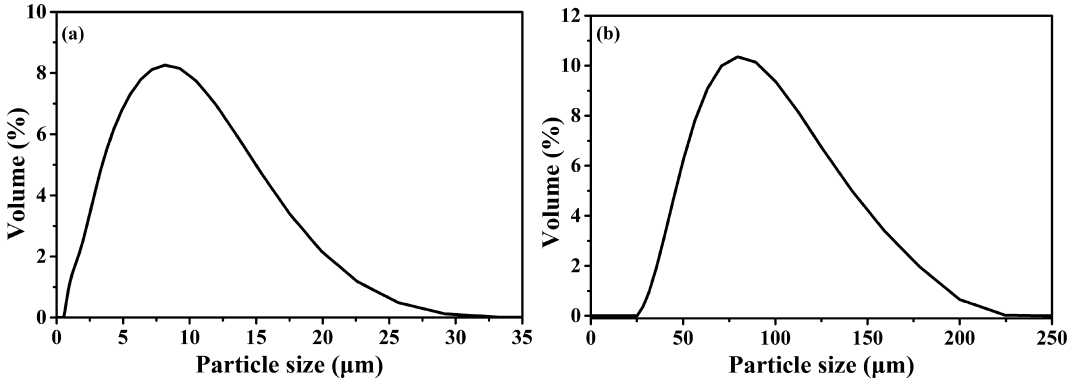

Fig. 1. The particle size distribution of the parent SAPO-34 crystal (a) and the SAPO-34 catalyst with binder mixed (b).

Table 1
Textural properties of parent SAPO-34 and SAPO-34-PC samples before and after MTO reaction for 2, 20, and 38 min.

Samples	Surface area ($m^2\ g^{-1}$)			Pore volume ($cm^3\ g^{-1}$)	
	S_{BET} [a]	S_{Micro} [b]	S_{Exter} [b]	V_{Micro} [b]	V_{Meso} [c]
SAPO-34	270	220	50	0.1	0.07
SAPO-34-PC	217	158	59	0.07	0.06
SAPO-34-2 min	253	197	56	0.09	0.07
SAPO-34-20 min	143	105	38	0.05	0.06
SAPO-34-38 min	81	36	45	0.02	0.06
SAPO-34-PC-2 min	197	139	58	0.06	0.07
SAPO-34-PC-20 min	96	57	39	0.03	0.06
SAPO-34-PC-38 min	59	13	46	0.01	0.07

[a] Total surface area is determined by the BET equation.
[b] Micropore surface area, external surface area, and micropore volume are calculated by the *t*-plot method.
[c] Mesopore volume is determined by the BJH method.

−92 ppm that is attributed to $Si(OAl)_4$, an isolated Si environment. An appreciable number of Si islands (i.e., $Si(OAl)_4$) that afford strong acid sites were not detected; this suggests a rather low probability for the highly active sites to play a significant role in the "precoking" reaction.

3.3. The effect of 1-butene "precoking" on the performance of the MTO reaction

The subsequent MTO reaction results are compiled in Fig. S4. "Precoking" treatment by 1-butene cracking for 2 min increased the initial ethene selectivity (MTO reaction for 2 min) from 27% for parent SAPO-34 to 43% for the "precoked" sample; extending the "precoking" duration to 10 min further enhanced the initial ethene selectivity to 56% but deactivated the catalyst quickly. Optimal MTO performance was achieved by adjusting the "precoking" time to 5 min, which yielded a high initial ethene selectivity, up to 50%, while maintaining the catalyst lifespan (Figs. 2 and S4). By doing so, olefin selectivity control would be no longer highly dependent on the age distribution of catalysts, which would beneficially extend the "optimal operation window" for industrial MTO operation [1]. We also attempted to calculate the "coke" selectivity roughly and the results are shown in Fig. S5. An SAPO-34 sample treated by 1-butene "precoking" for 5 min, abbreviated as SAPO-34-PC, was selected as the typical catalyst for the following mechanistic study.

3.4. The spatial location of the presituated "coke"

1-Butene "precoking" treatment exerted a marginal effect on the crystallinity of SAPO-34 (Fig. S6). Yet careful inspection of its

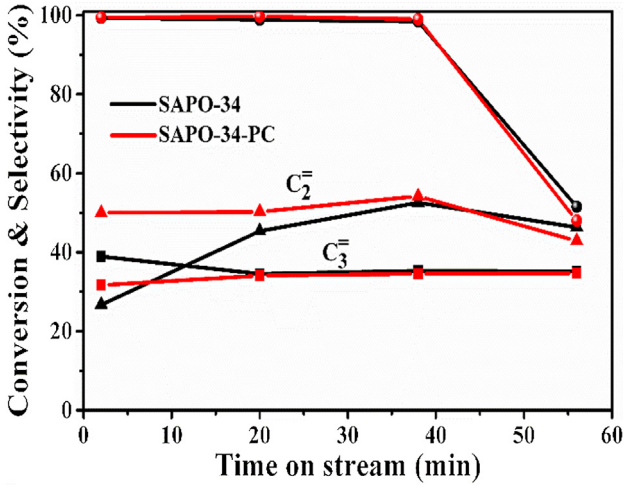

Fig. 2. The methanol conversion and ethene and propene selectivities of the MTO reaction over SAPO-34 and SAPO-34-PC ("precoking" for 5 min) at 490 °C with WHSV of 5 h^{-1}.

XRD pattern indicates a peak shift toward lower angles, implying the expansion of the zeolite lattice induced by "coke" deposition into the internal pores of SAPO-34 [32,33]; this is ascertained by the Pawley analysis (from the profile fitting of the XRD patterns shown in Fig. S7) that shows the unit cell parameters being expanded after preseeding of "coke" (SAPO-34: $a = b = 13.63$, $c = 14.84$; SAPO-34-PC: $a = b = 13.67$, $c = 14.92$). After 1-butene "precoking" treatment, the micropore surface area and volume decreased by 32% and 29%, respectively (Table 1). However, the mesopore volume remained unchanged (Table 1 and Fig. S8). This observation directly evidences that the presituated "coke" is localized in the internal pores of SAPO-34, thus excluding the possible effect of external surface coking on the subsequent MTO reaction. Naphthalene was identified by GC–MS analysis as the dominant aromatic species occluded in the pores of SAPO-34 (Fig. 3a). The specificity for 1-butene to form naphthalene agrees qualitatively with previous reports that the smaller ethene molecule is inclined to form multicyclic aromatics with three to four rings, yet the larger 1-butene molecule prefers to produce lighter aromatics [34,35]. The cage occupancy by naphthalene was estimated by internal standard to be ca. one molecule per 18 cages. Naphthalene was suggested to reside relatively homogeneously across the SAPO-34 crystal (Fig. 3b), as deduced from careful analyses of the product pattern of 1-butene cracking as well as the Si environment probed by ^{29}Si MAS NMR as discussed above; this plausible conclusion was further solidified by the experimental evidence of FTIR and isotopic labeling, as discussed in the following section.

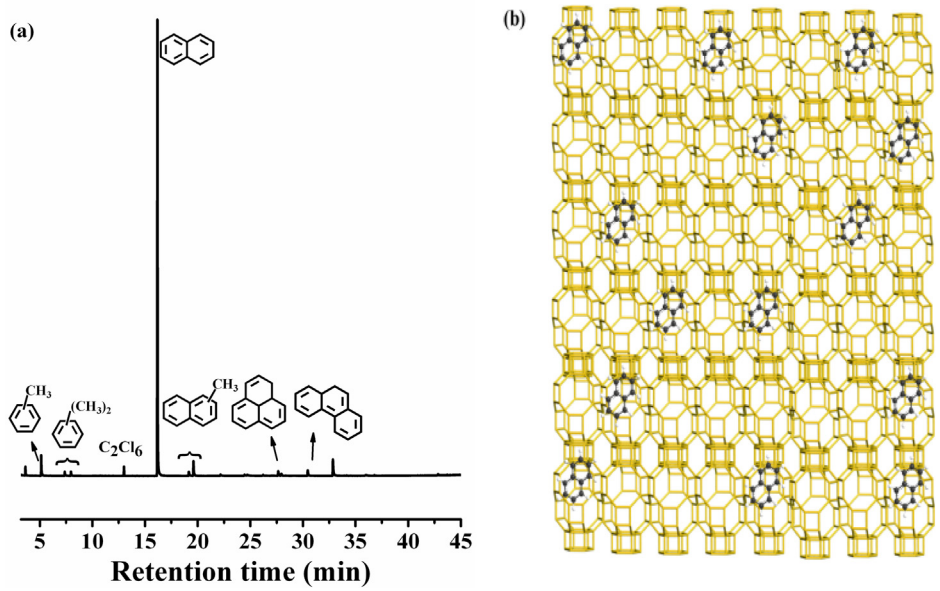

Fig. 3. GC–MS analysis of the retained aromatics in the SAPO-34 sample (a) and the uniform spatial distribution of naphthalene as the main pre-situated "coke" species after 1-butene "precoking" treatment (b).

3.5. The impact of "coke" location on acid site utilization and the MTO reaction performance

Different from the case of the "precoking" reaction, a spectrum of the pore-entrapped aromatic species ranging from methylbenzene to pyrene derivatives was observed over both parent and "precoked" SAPO-34 after the MTO reaction. The relationship between micropore volume and the content of "coke" is presented in Fig. S9. The micropore volume was found to decrease almost linearly with "coke" content for both SAPO-34 and SAPO-34-PC samples, ruling out external surface coking and suggesting that the MTO reaction was largely localized inside the internal pores of SAPO-34, at least for TOS < 38 min. We also theoretically estimated the relationship between micropore volume and "coke" content by assuming "coke" density to be 1.2 g/cm^3 [36] and plotted this trend as the dashed line in Fig. S9. If the micropore volume decreases more slowly than the theoretical estimate (that is, the measured line runs above the estimated one), external surface coking will occur [36]. But almost comparable (in the initial stage) and relatively slower decline (considering that the actual "coke" density may deviate from the assumed constant value) of micropore volume relative to theoretical estimate, again demonstrating that "coke" buildup during the MTO reaction under the applied reaction conditions occurs exclusively inside the micropores of the SAPO-34 crystal. The conclusion arrived at here serves as a prerequisite for interpreting the proposed reaction pattern sketched in Scheme 1 mechanistically.

The "coke" deposition and the induced restriction in mass transfer may have both detrimental and promotional effects on the MTO reaction. The optimization of 1-butene "precoking" parameters is associated with the modulation of "coke" molecules, involving the amounts and the spatial location (in the micropores or at the external surface; localized at the rim cages or homogenously distributed in the cage-structured zeolites). Occluded heavier aromatic compounds can, on one hand, hinder the diffusion of molecules and eventually block pores of zeolites [37], and on the other hand, have a promoting effect on MTO turnover [13,37,38]. Going with the gradual "coke" deposition is the advent of diffusion hindrance on the molecules present in zeolitic pores. In addition to the deleterious effect on catalytic activity, retarded diffusion for certain intermediates may induce a positive effect as well, such as by preventing the active aromatics from diffusing out of the HZSM-5 channel, which benefits ethene formation [39], by providing opportunities for abundant yet less active tetramethylbenzene, which is subject to subsequent methylation reaction, to form a more active pentamethylbenzenium intermediate on ZSM-12 [40].

The "coke" amount determined by TGA was linearly dependent on TOS (Fig. 4a). Upon subtraction of the amount of presituated "coke" (3.5 wt%), the SAPO-34-PC sample exhibited a lower mass-specific "coke" deposition rate of 1.4 mg min^{-1} than the parent sample with a rate of 1.7 mg min^{-1}. This points to an intriguing finding that evenly settling a certain amount of carbonaceous species into SAPO-34 cages prior to MTO reaction can effectively decelerate "coke" deposition; this can be explained by the attenuated local methanol concentrations (due to the extending of reaction zone inward of crystal as discussed below) and resultantly more lighter aromatics occluded on SAPO-34-PC than on the parent SAPO-34 (Fig. 5). It is worth recalling that the ethene selectivity over SAPO-34-PC was almost invariable with TOS, in contrast with the case of the parent sample, for which the ethene selectivity increased monotonically with the "coke" accumulation (Figs. 2 and S4). This implies that a definitive relation between "coke" content and ethene selectivity does not exist. For instance, the ethene selectivity of 50% after MTO reaction for 2 min over SAPO-34-PC was close to the 52% for pristine SAPO-34 after 38 min of reaction (Fig. 2), with the former yielding 4.7 wt% "coke" while the latter giving 7.7 wt% "coke." In other words, comparable ethene selectivity can be achieved with quite different amounts of "coke," highlighting the importance of "coke" location. Moreover, 3.5 wt% of predeposited "coke" corresponds roughly to the "coke" amount attained after MTO reaction for around 13 min (estimated from Figs. 2 and 4a) for parent SAPO-34. If we assume that such predeposited "coke" was localized in the periphery cages of SAPO-34, ethene selectivity will keep increasing with TOS, in a manner similar to that for parent SAPO-34, as shown in Fig. 2. This reasoning, again, highlights the importance of evenly spatial siting of "coke."

Fig. 4b compares the IR spectra of SAPO-34 and SAPO-34-PC before and after the MTO reaction in a range showing the stretching vibrations of OH groups. The peaks at 3740 and 3680 cm^{-1} are ascribed to the Si—OH and P—OH groups, respectively; the two

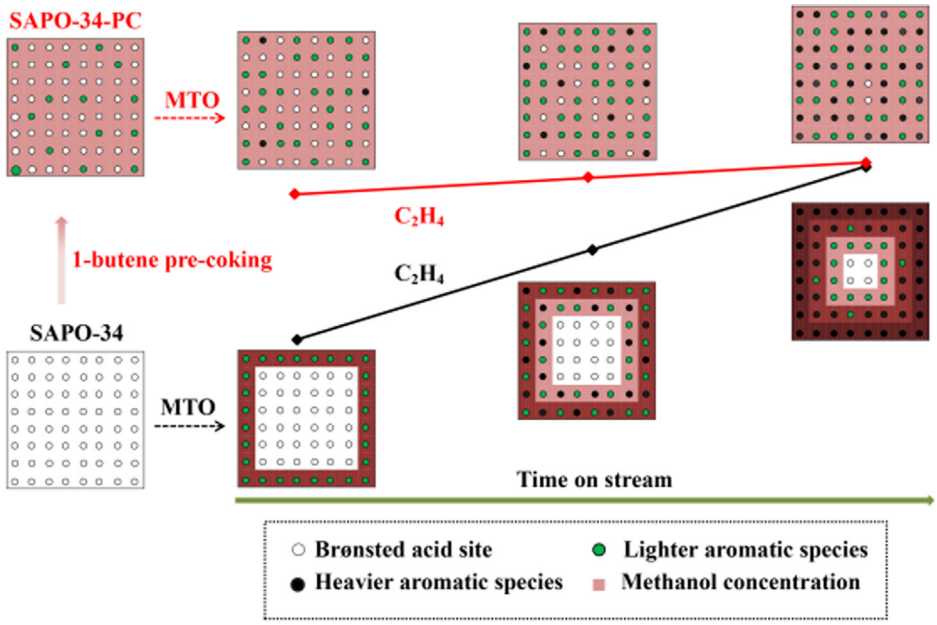

Scheme 1. Schematic illustration of the normal MTO reaction pattern (bottom) and the effect of the presituated "coke" on the MTO reaction (up).

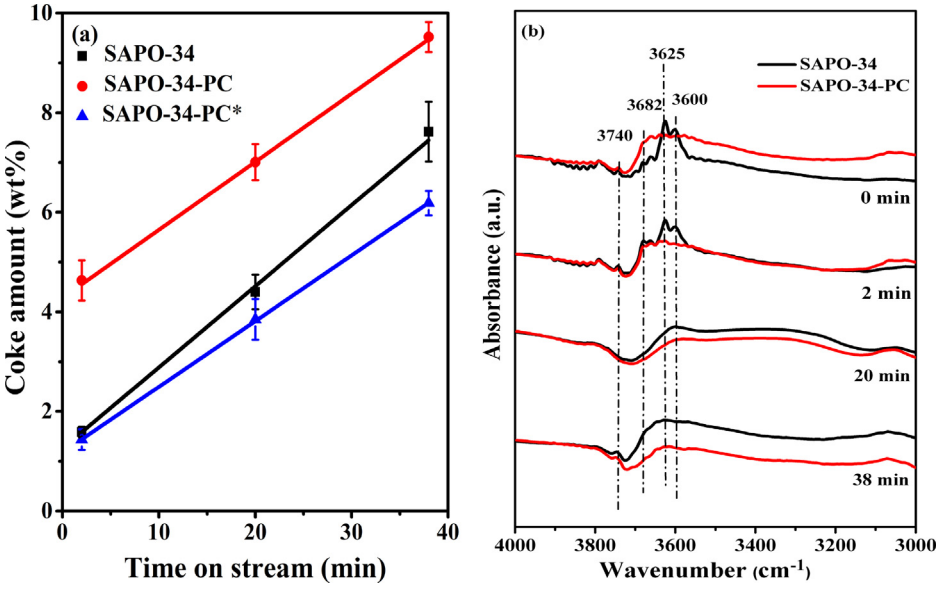

Fig. 4. The "coke" amount (a) and FTIR spectra (b) of SAPO-34 and SAPO-34-PC samples with MTO reaction. * represents the "coke" content of the SAPO-34-PC sample after subtraction of the presituated "coke" (3.5 wt%) from the 1-butene cracking process.

intense bands centered at 3600 and 3625 cm^{-1} are assigned to acidic Si—OH—Al [41]. It is shown that the cumulative "coke" with TOS progressively covered the Brønsted acid sites (BAS), as reflected by the steady attenuation of peaks at 3600 and 3625 cm^{-1}. Noteworthily, the BAS of SAPO-34-PC always decreased more obviously than that of the parent SAPO-34, regardless of the reaction's proceeding. In addition, the respective variation of BAS amounts probed by NH_3 IR (as shown in Table S2) are highly consistent with this observation. Even though the presituated "coke" would occupy a portion of the BAS, much more "coke" was accommodated on SAPO-34-PC than on SAPO-34 (Fig. 4a) and the catalyst lifetimes for the catalysts were almost comparable (or the catalyst lifetime for SAPO-34-PC was slightly shortened; Fig. 2); this leads us to deduce that the "precoking" treatment aids in efficient utilization of the BAS. This conclusion agrees well with the methanol uptake results measured by TGA, as shown in Fig. S10. The enhanced utilization efficiency of the BAS may be a result of the relatively uniform distribution of presituated "coke" that facilitates the extension of the reaction zone inward.

3.6. The plausibility of product shape selectivity, transition-state shape selectivity, and methylnaphthalene species as causes for the increase in ethene selectivity

The product shape selectivity induced by the configurational diffusion of products was often considered as one main reason

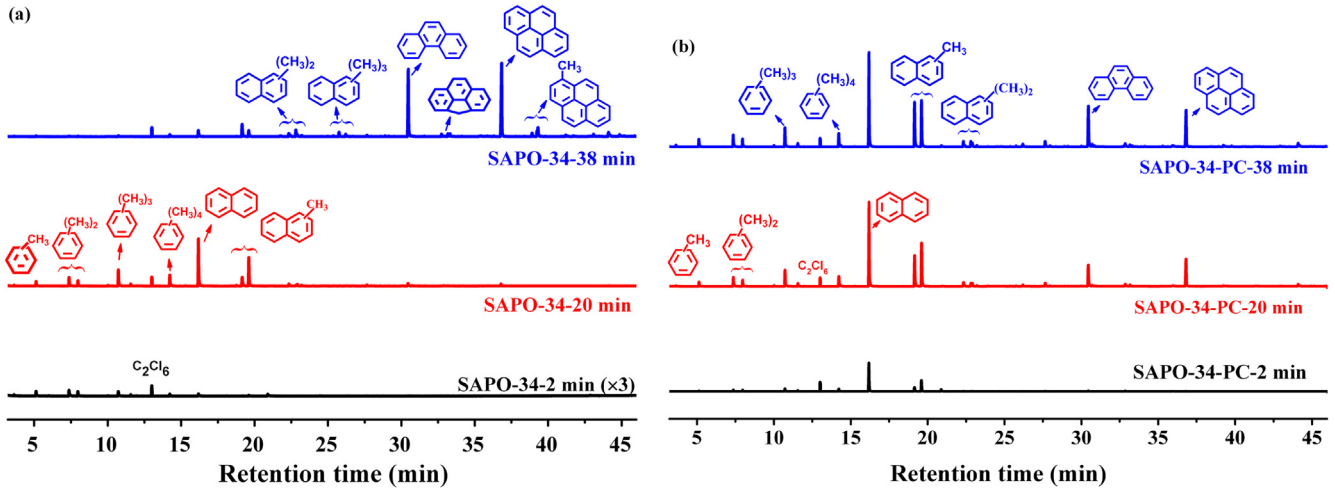

Fig. 5. GC–MS analysis of the evolution of the retained aromatics with TOS for the MTO reaction for parent SAPO-34 (a) and SAPO-34-PC (b) samples. Detailed views of the locally magnified lines, including the peak of hexaMB, are shown in Fig. S11 for both samples.

Table 2
The D_s of ethene, propene, and 1-butene on AlPO-34 catalyst at different temperatures and the D_s ratio of these three molecules.

D_s (10^{-12} m^2 s^{-1})	Temperature			D_s ratio	Temperature		
	27 °C	290 °C	490 °C		27 °C	290 °C	490 °C
C_2H_4	18.2	157.9	368.8	C_2H_4/C_3H_6	33	12	10
C_3H_6	0.56	13.2	36.9	C_2H_4/C_4H_8	—	150	91
C_4H_8	—	1.05	4.06	C_3H_6/C_4H_8	—	13	9

Note: AlPO-34 (the counterpart of SAPO-34 without BAS) model was adopted here to simplify the calculation system.

for explaining ethene increase [5,14]. The self-diffusion coefficients (D_s) of ethene, propene, and 1-butene molecules were estimated by MD calculations at 27, 290, and 490 °C, respectively (Table 2). At each temperature, a noticeable reduction in the diffusion coefficient from ethene to 1-butene was observed, reflecting the greater diffusional hindrance for bulky olefin molecules. It can be deduced rationally that the catalyst with "coke" deposition would be likely to hinder the diffusion of olefinic species, especially for bulky olefin molecules. While high temperature would tend to mitigate the diffusional discrimination between ethene, propene, and 1-butene, the diffusion coefficient of propene was still found to be 10 times lower than that of ethene at 490 °C (the temperature applied for industrial MTO processes). Hence, if product shape selectivity plays the decisive role in controlling the product distribution, parallel to the progressive increase in ethene selectivity with TOS (that is, with gradual "coke" deposition) for parent SAPO-34, propene and C_4^+ products should decrease greatly. However, a reduction in propene selectivity was observed in the MTO reaction for only 2 min and then propene became insensitive to the progress of reaction (Fig. 2). As for the "precoked" SAPO-34, the selectivity to both ethene and propene increased slightly with TOS (Figs. 2 and S4), although significant amounts of "coke" were deposited steadily inside the cavities of SAPO-34 (Fig. 4a) that would severely hinder the diffusion of propene than ethene. These analyses allow us to conclude that ethene increase cannot be simply ascribed to product shape selectivity.

The lighter aromatic species, such as xylene and triMB, have been considered as the active species responsible for ethene formation on both SAPO-34 [15] and HZSM-5 [42]. GC–MS analysis of the retained aromatics (Fig. 5) shows that the relative abundance of xylene and triMB increased with TOS for both samples, especially for SAPO-34-PC, coinciding with the increase in ethene selectivity (Fig. 2). Besides, the pore volume of SAPO-34 shrank remarkably with the progress of the reaction (Table 1). Based on these analyses, one may presume that ethene increase might originate from a shift of active species from heavier methylbenzenes to lighter ones, that is, due to the transition-state shape selectivity, with xylene and triMB acting as the key contributors for ethene increase as described by the previous reports [13,15,42]. The incorporation of ^{13}C atoms into hydrocarbons determined by ^{12}C-/^{13}C-methanol switch experiments was perceived as an indicator for discriminating the active intermediates from the spectators and for evincing the genesis of products [5]. As shown in Figs. 6a and 6c, the ^{13}C content of methylbenzenes decreased with the reduction in methyl group substitution, in accordance with the observations for H-β [43] but in contrast to the results for HZSM-5 [3,43]. This observation obviously demonstrates that hexaMB acts invariably as the most active intermediate throughout the entire MTO reaction for both pristine and "precoked" SAPO-34. This allows us to conclude unequivocally that the transition-state shape selectivity is not the main cause for ethene increase. Apart from this, the quick decrease in isotopic scrambling for triMB and the always low ^{13}C content for xylene on parent SAPO-34 with the increase of TOS (Fig. 6a), together with the rather lower activity of triMB and xylene on SAPO-34-PC (Fig. 6c), lead undoubtedly to the information that ethene increase is independent of the content of triMB and xylene, again disproving the possibility of transition-state shape selectivity.

It was previously reported that methylnaphthalene has a propensity to form ethene [16]. Naphthalene and methylnaphthalene species dominated the extracts for SAPO-34-PC throughout the entire reaction stages, as shown in Fig. 5b. This observation may partly relate to the abundant retained naphthalene species being generated during the "precoking" stage (Fig. 3), but more relevantly, it is presumed that these increased naphthalene species were formed during the MTO reaction, on the basis of the

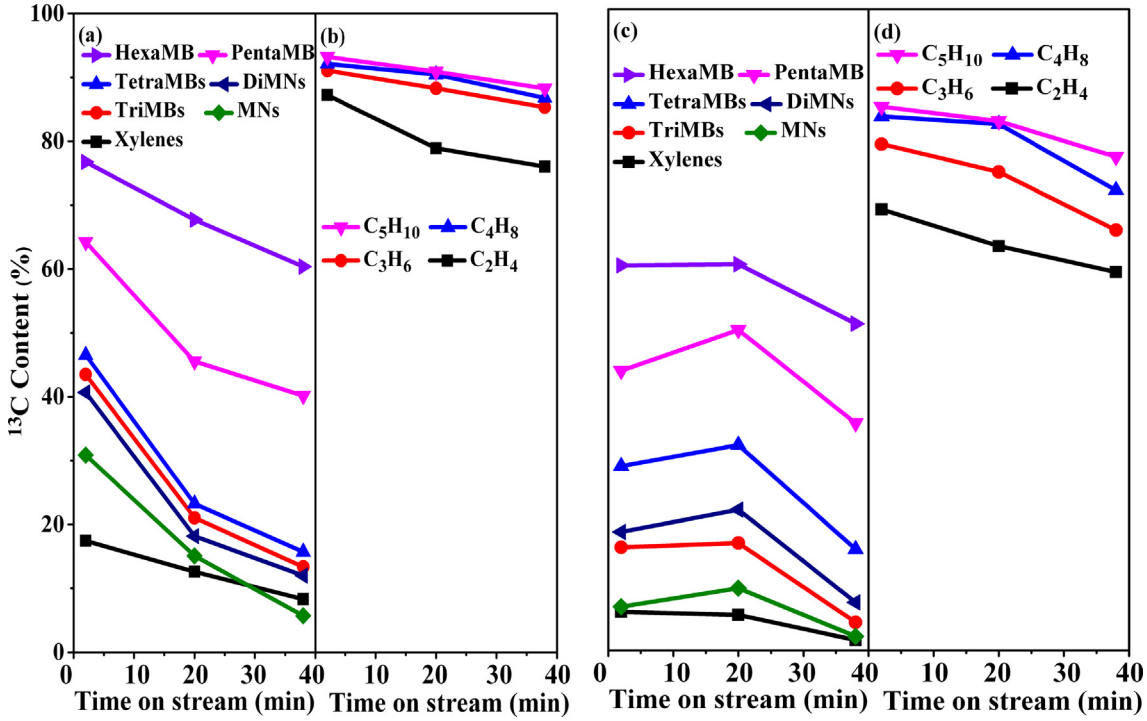

Fig. 6. The total ^{13}C content of the retained aromatics (a and c) and effluent olefins (b and d) obtained by ^{12}C-/^{13}C-methanol switch experiments at 490 °C over SAPO-34 (a and b) and SAPO-34-PC (c and d) with ^{12}C-methanol feeding for 2, 20, and 38 min, respectively, followed by 10 s of ^{13}C-methanol feeding. The isotopic distribution in the effluent olefins and the retained aromatics is provided in Fig. S12. MNs and DiMNs represent monomethylnaphthalene and dimethylnaphthalene, respectively.

extension of the reaction zone inward of the crystal and thus more BAS being utilized (as discussed before). It seems plausible to correlate the ethene increase with methylnaphthalene speciation. Nevertheless, of particular note was that upon 38 min reaction, phenanthrene and pyrene constituted the main retained compounds over SAPO-34, in contrast to the prevalence of naphthalene and its derivatives for SAPO-34-PC. Almost equivalent ethene selectivity was achieved for both catalysts after 38 min of MTO reaction. This implies that methylnaphthalene species would not be the main contributor to ethene increase. Furthermore, the isotopic content of methylnaphthalene over parent SAPO-34 was around 30–40% after 2 min of MTO reaction, but it decreased quickly to 20% after 20 min reaction (Fig. 6a), the trend of which is opposite to the ethene increase profile. This, along with the large decrease in ^{13}C incorporation for naphthalene derivatives over SAPO-34-PC (Fig. 6c), demonstrates that methylnaphthalene species may contribute to ethene formation to some extent, but could not serve as the main cause for ethene increase. It is added that in the original work that initially reported methylnaphthalenes yielding higher ethene selectivity, the authors also stressed that the reactivity of methylnaphthalene was temporary and would be quickly masked by other active species (i.e., methylbenzenes) [16].

3.7. The mechanistic origin of the increase in ethene selectivity

Different from the deactivation mode of HZSM-5 (i.e., external surface coking [44]), shell deactivation usually occurs for SAPO-34 with unique "coke" filling within the near-surface shell cages [18,20], which would obstruct the internal BAS from being effectively accessed and utilized [20]. The ^{13}C-incorporation of the retained aromatics decreased rapidly with TOS for the parent SAPO-34 (Fig. 6a). This implies that the confined HCP species, initially generated at the outer rim of the crystal, hamper the access of active aromatic intermediates to reactant methanol molecules. After "precoking" treatment, the isotopic scrambling for aromatic species decreased obviously after MTO reaction for 2 min compared to that for parent SAPO-34 (Fig. 6c). However, ^{13}C-incorporation after 20 min reaction was found to be identical to, or slightly higher than, that after 2 min reaction for SAPO-34-PC. This distinct observation suggests that the diffusional restriction on methanol has been significantly alleviated by the even distribution of the presituated "coke." As a result, the MTO reaction is no longer localized at the shell layer of cavities of SAPO-34 but is extended toward the interior of the crystal (that is, the local methanol concentrations are attenuated); this corresponds to prolonging of diffusion length and/or enlargement of effective crystallite size. The similar case was found for HZSM-5 after silylation treatment that enlarged the effective crystalite size [7].

Figs. 6b and 6d additionally show that the ^{13}C content for ethene was distinct from that for C_3–C_5 alkenes, but the ^{13}C incorporation for olefins was always higher than that for aromatics. These observations suggest the presence of olefins-based cycles (except for the aromatics-based cycle) on both SAPO-34 and SAPO-34-PC samples under the reaction conditions studied (490 °C), in contrast with the sole operation of the aromatics-based cycle at 350 °C [5]. The parallel propagation of olefins- and aromatics-based cycles would generate more olefinic intermediates. However, in view of the one order of magnitude higher diffusion coefficient of propene than 1-butene (Table 2), the increased diffusion length of molecules would moderately hinder the diffusion of propene but would significantly inhibit the diffusion of C_4^+ products. This explains the almost invariable propene selectivity and the gradually decreased C_4^+ product selectivity with TOS (Figs. 2 and S4). As for SAPO-34-PC, the selectivity of C_4^+ products (the main constituents of which were olefins) was lower than that for parent SAPO-34, especially in the early reaction stage (Fig. S4). The reason lies in the extension of the reaction zone (i.e., increased diffusion length) which hampers the bulkier products from diffusing out. These retained olefinic species, being subject to a longer intracrystalline residence time, would subsequently be consumed via the

consecutive condensation and H-transfer reactions, yielding more (lighter) aromatic species (see Fig. 5). This reasoning was also directly supported by the finding that more C_3–C_5 alkanes (formed via H-transfer reaction) were occluded in the "precoked" SAPO-34 after the MTO reaction, as evidenced by the GC–MS results shown in Fig. S13 as well as the FTIR analysis shown in Fig. S14. Eventually, the largely formed active aromatic species would generate more ethene via the aromatics–ethene route.

Although ethene has been proposed [3,4] and substantiated [7] as the product of an aromatics-based cycle, the higher ^{13}C content in ethene relative to the most active aromatic (hexaMB) (Fig. 6) clearly suggests that ethene, besides being produced from an aromatics-based cycle (where the side-chain methylation mechanism may contribute to higher ^{13}C content in view of the successive methylation with ^{13}C-labeled methanol), is also a product of an olefins-based cycle. This prominent distinction (relative to literature results [3,4,7]) lies in the different reaction conditions applied; a high temperature up to 490 °C was applied in this work while a low temperature of 350 °C was used in the literature [3,4,7]. The higher temperature applied here would facilitate the partial cracking of higher olefins to ethene, a conclusion reached with theoretical and experimental evidence in the literature [8,45,46]. Ethene has been ascertained to be rather less reactive than C_3^+ olefins [47,48] and was shown to diffuse much more easily than propene and butene (Table 2), thus behaving as an end product without itself getting consumed before exiting the pores of SAPO-34.

With regard to the parent SAPO-34, the MTO reaction zone tends to evolve from the exterior to the inner part of the SAPO-34 crystal [18,20] (as shown in Scheme 1); the reaction/diffusion path is concurrently increased with TOS. So the gradual increase of ethene selectivity with TOS for the parent SAPO-34 (Fig. 2) could also be explained by the consequences of the extension of the reaction into the core of the crystal.

A comparison of the normal MTO reaction pattern for SAPO-34 and the effect of the presituated "coke" on the spatial distribution of HCP species and then the ethene selectivity is sketched in Scheme 1. The 1-butene "precoking" technology presented here is expected to be transferable to other olefins and hydrocarbons, but beyond the scope of the present contribution.

4. Conclusions

In summary, this work presents a facile 1-butene "precoking" strategy to unprecedentedly enhance the ethene selectivity without affecting the catalyst lifetime. The "precoking" strategy developed here holds great promise for the MTO industry. The increased ethene partly originates from the olefin methylation-cracking route, and more relevantly, the extension of the reaction zone inward in the crystal (due to the evenly distributed presituated "coke" from 1-butene cracking) facilitates the aromatics–ethene route. The discrimination of reactivity and diffusional behavior for different olefins finally sieves the most diffusional ethene as the major end product at the expense of higher olefins. The mechanistic understanding here underscores the importance of tailoring the catalytic microenvironment of the zeolite by controlling "coke" spatial siting in modulating the product selectivity; this would help in opening new avenues for orientable conversion of methanol and other organic compounds.

Acknowledgments

The authors thank the National Natural Science Foundation of China (Grant 21703239 and 91334205), the Key Research Program of Frontier Sciences of Chinese Academy of Sciences (Grant QYZDY-SSW-JSC024), and the International Partnership Program of Chinese Academy of Sciences (Grant 121421KYSB20180007) for financial support. The authors declare no competing financial interest.

Appendix A. Supplementary material

Supplementary data to this article can be found online at https://doi.org/10.1016/j.jcat.2019.06.014.

References

[1] P. Tian, Y.X. Wei, M. Ye, Z.M. Liu, ACS Catal. 5 (2015) 1922–1938.
[2] X.S. Yuan, H. Li, M. Ye, Z.M. Liu, Chem. Eng. J. 329 (2017) 35–44.
[3] S. Svelle, F. Joensen, J. Nerlov, U. Olsbye, K.P. Lillerud, S. Kolboe, M. Bjørgen, J. Am. Chem. Soc. 128 (2006) 14770–14771.
[4] M. Bjørgen, S. Svelle, F. Joensen, J. Nerlov, S. Kolboe, F. Bonino, L. Palumbo, J. Catal. 249 (2007) 195–207.
[5] B.P.C. Hereijgers, F. Bleken, M.H. Nilsen, S. Svelle, K.P. Lillerud, M. Bjørgen, B.M. Weckhuysen, U. Olsbye, J. Catal. 264 (2009) 77–87.
[6] S. Wang, Y.Y. Chen, Z.H. Wei, Z.F. Qin, H. Ma, M. Dong, J.F. Li, W.B. Fan, J.G. Wang, J. Phys. Chem. C 119 (2015) 28482–28498.
[7] R. Khare, D. Millar, A.A. Bhan, J. Catal. 321 (2015) 23–31.
[8] X. Sun, S. Mueller, Y. Liu, H. Shi, G.L. Haller, M. Sanchez-Sanchez, A.C. Van-Veen, J.A. Lercher, J. Catal. 317 (2014) 185–197.
[9] J.W. Zhong, J.F. Han, Y.X. Wei, S.T. Xu, Y.L. He, M. Ye, X.W. Guo, C.S. Song, Z.M. Liu, Chem. Commun. 54 (2018) 3146–3149.
[10] H. Schulz, M. Wei, Micropor. Mesopor. Mater. 29 (1999) 205–218.
[11] H. Schulz, Catal. Lett. 148 (2018) 1263–1280.
[12] I. Yarulina, A.D. Chowdhury, F. Meirer, B.M. Weckhuysen, J. Gascon, Nat. Catal. 1 (2018) 398–411.
[13] D. Chen, K. Moljord, T. Fuglerud, A. Holmen, Micropor. Mesopor. Mater. 29 (1999) 191–203.
[14] I.M. Dahl, R. Wendelbo, A. Andersen, D. Akporiaye, H. Mostad, T. Fuglerud, Micropor. Mesopor. Mater. 29 (1999) 159–171.
[15] W.G. Song, H. Fu, J.F. Haw, J. Am. Chem. Soc. 123 (2001) 4749–4754.
[16] W.G. Song, H. Fu, J.F. Haw, J. Phys. Chem. B 105 (2001) 12839–12843.
[17] S.T. Xu, Y.C. Zhi, J.F. Han, W.N. Zhang, X.Q. Wu, T.T. Sun, Y.X. Wei, Z.M. Liu, Adv. Catal. 61 (2017) 37–122.
[18] Q.Y. Qian, J. Ruizmartínez, M. Mokhtar, A.M. Asiri, S.A. Althabaiti, S.N. Basahel, V.D.B. He, J. Kornatowski, B.M. Weckhuysen, Chem. Eur. J. 19 (2013) 11204–11215.
[19] J.C. Groen, L.A.A. Peffer, J. Pérez-Ramírez, Micropor. Mesopor. Mater. 60 (2003) 1–17.
[20] Z.J. Wan, G.K. Li, C.F. Wang, H. Yang, D.K. Zhang, Appl. Catal. A Gen. 549 (2018) 141–151.
[21] P. Magnoux, P. Roger, C. Canaff, V. Fouche, N.S. Gnep, M. Guisnet, Stud. Surf. Sci. Catal. 34 (1987) 317–330.
[22] C. Baerlocher, L. B. McCusker, Database of Zeolite Structures, available at http://www.iza-structure.org/databases/. Accessed June 2016.
[23] J.D. Gale, J. Phys. Chem. B 28 (1998) 5423–5431.
[24] M.J. Sanders, M. Leslie, C.R.A. Catlow, J. Chem. Soc. Chem. Comm. 19 (1984) 1271–1273.
[25] C.D. Wick, M.G. Martin, J.I. Siepmann, J. Phys. Chem. B 104 (2000) 8008–8016.
[26] J.C. Palmer, J.D. Moore, T.J. Roussel, J.K. Brennan, K.E. Gubbins, Phys. Chem. Chem. Phys. 13 (2011) 3985–3996.
[27] W. Smith, T.R. Forester, J. Mol. Graph. 14 (1996) 136–141.
[28] D. Frenkel, S. Berend, Understanding Molecular Simulations, Academic Press, San Diego, 2002.
[29] X.P. Tang, H.Q. Zhou, W.Z. Qian, D.Z. Wang, Y. Jin, F. Wei, Catal. Lett. 125 (2008) 380–385.
[30] D. Chen, H.P. Rebo, K. Moljord, A. Holmen, Stud. Surf. Sci. Catal. 111 (1997) 159–166.
[31] U.V. Mentzel, S. Shunmugavel, S.L. Hruby, C.H. Christensen, M.S. Holm, J. Am. Chem. Soc. 131 (2009) 17009–17013.
[32] M. Zokaie, D.S. Wragg, A. Gronvold, T. Fuglerud, J.H. Cavka, K.P. Lillerud, O. Swang, Micropor. Mesopor. Mater. 165 (2013) 1–5.
[33] J. Goetze, I. Yarulina, J. Gascon, F. Kapteijn, B.M. Weckhuysen, ACS Catal. 8 (2018) 2060–2070.
[34] E. Epelde, M. Ibañez, A.T. Aguayo, A.G. Gayubo, J. Bilbao, P. Castaño, Micropor. Mesopor. Mater. 195 (2014) 284–293.
[35] B. Hu, G.L. Mao, D.K. Wang, Y.D. Fu, B.H. Wang, M.J. Luo, Catal. Sci. Technol. 7 (2017) 5785–5794.
[36] D.M. Bibby, N.B. Milestone, J.E. Patterson, L.P. Aldridge, J. Catal. 97 (1986) 493–502.
[37] D. Chen, K. Moljord, A. Holmen, Micro. Mesopor. Mater. 164 (2012) 239–250.
[38] Y.X. Wei, D.Z. Zhang, F.X. Chang, Q.H. Xia, B.L. Su, Z.M. Liu, Chem. Commun. 34 (2009) 5999–6001.
[39] R. Khare, B. Aditya, J. Catal. 329 (2015) 218–228.
[40] Z.Q. Liu, Y.Y. Chu, X.M. Tang, L. Huang, G.C. Li, X.F. Yi, A.M. Zheng, J. Phys. Chem. C 121 (2017) 22872–22882.
[41] Y.X. Wei, D.Z. Zhang, Z.M. Liu, B.L. Su, J. Catal. 238 (2006) 46–57.

[42] C. Wang, J. Xu, G.D. Qi, Y.J. Gong, W.Y. Wang, P. Gao, Q. Wang, N.D. Feng, X.L. Liu, F. Deng, J. Catal. 332 (2015) 127–137.
[43] S. Svelle, U. Olsbye, A.F. Joensen, M. Bjørgen, J. Phys. Chem. C. 111 (2007) 17981–17984.
[44] D. Mores, E. Stavitski, M.H.F. Kox, J. Kornatowski, U. Olsbye, B.M. Weckhuysen, Chem. Eur. J. 14 (2008) 11320–11327.
[45] W. Wu, W. Guo, W. Xiao, M. Luo, Chem. Eng. Sci. 66 (2011) 4722–4732.
[46] C.M. Wang, Y.D. Wang, Z.K. Xie, J. Catal. 301 (2013) 8–19.
[47] I.M. Dahl, S. Kolboe, J. Catal. 149 (1994) 458–464.
[48] A. Hwang, D. Prieto-Ceturion, A. Bhan, J. Catal. 337 (2016) 52–56.